Comparison of Creep Behaviour of UD and Woven CFRP in Bending

Rui Miranda Guedes and Mário A. Vaz

Department of Mechanical Engineering and Industrial Management (DEMEGI), Faculty of Engineering of University of Porto (FEUP), Rua dos Bragas, 4050-123 PORTO, PORTUGAL

Abstract. The experimental results for creep bending tests of tape and twill woven CFRP laminates are presented and discussed. The aim of the research programme was to characterise and compare the long-term behaviour of both laminates. These materials will be included as structural elements in the construction of supports for delicate and precise radiation detection elements, so, they need to be highly stable under any environmental conditions. The time dependency of the fibre-dominated properties of the CFRP laminates is negligibly small. Therefore the initial analysis pointed to a better creep behaviour of the twill woven CFRP laminate and also predicted null creep strains. The experimental results shown a different picture, the tape laminates performed better than the woven laminates, which exhibit larger creep strains than the initial guess.

Introduction

The European Laboratory for Particle Physics (CERN) is building a new particle accelerator called LHC (Large Hadron Collider). The LHC is an accelerator that brings protons and ions into head-on collisions at higher energies than ever achieved before. This will allow scientists to penetrate still further into the structure of matter and recreate the conditions prevailing in the early universe, just after the "Big Bang". This is a big project with

new challenges in many engineer fields, especially in the application of new materials. The DEMEGI-INEGI group is involved in the characterisation of advanced composite materials that will be used to build the support structures of particle detectors. These structures should present a high dimensional stability because small deviations from the initial position will lead to large errors in signal detection of the particles. A research program was established to determine the long-term behaviour of two different composite materials. Environment controlled bending creep tests of cantilever plates were used in order to compare the behaviour of two different CFRP (Carbon Fibre Reinforced Polymers). Although bending tests do not produce uniform stresses and strains in the material and introduce, simultaneously, creep in bending and in plane stress relaxation, they are easier to perform than the tensile tests. Nevertheless the research team acquired some experience in this type of tests [1] with satisfactory results in recent years. On the other hand bending loads are present in almost every real structure and are difficult, if not impossible, to avoid.

In design, when creep is considered, it is usual that the item should remain in service for an extended time, usually longer than it is practical to run creep experiments on the material to be employed. Thus, it is necessary to extrapolate the information,obtained from relatively short time laboratory creep tests, applying the Time-Temperature-Superposition Principle (TTSP) to predict the in-service behaviour. Therefore this work is also a contribution to assess the application of TTSP as a basis for a long-term behaviour prediction.

Material

A brief presentation of the experimental test specimens is given. A set of 50x200mm2 specimens was obtained from composite plates fabricated at INEGI using the unidirectional UC125 RNA and the twill woven CC194 RNA. The resin epoxy system (RNA) was the same for both laminates having a 125^o C cure-temperature. The stacking sequence of the laminates and the geometry of test specimens presented in tables 1, 2 and 3 where B represents the width and h the thickness of each one.

Mechanical characterisation

The layer elastic properties had been already determined at the INEGI by conventional tests. The table 4 summarises the results obtained for the two laminates.

The 3 point bending flexural test, as shown in figure 1, was used to determine the bending modulus (E_b) and the bending stress strength (σ_r).

The geometry of the test follows the ASTM D790M standard except for the rate definition. In these tests a rate of 5mm/min was used instead of 12mm/min recommended by the standard. The stiffness to strength ratio and the geometry of the laminates was chosen in order to obtain large deflections in 3PB tests. The ASTM standard recommends the following formula to determine the rupture stress:

$$\sigma_r = \frac{3P \cdot L}{2B \cdot h^2} \left[1 + 6 \left(\frac{w_{\max}}{L} \right) - 4 \left(\frac{h \cdot w_{\max}}{L^2} \right) \right] \tag{1}$$

In this formula σ_r = rupture stress in outer fibres at midspan; P = load at break; L = load span; B = width of the beam; h = thickness of the beam; w_{max} = deflection at the centre of the span.

There is an exact solution for the large deflection of a simply supported beam with a central load [2], although an iterative numerical method is needed to obtain the solution due to the non-linear nature of the exact solution. On the other hand an approximated solution was obtained based on the classical beam theory, denominated from now on as corrected linear theory (CLT).

The corrected bending moment at any cross section of the beam, using the referential system given in figure 2, is

$$M = -\frac{P}{2}x - N \cdot y \quad , \tag{2}$$

with

$$\begin{cases} N = R\sin(\alpha) \\ R\cos(\alpha) = \frac{P}{2} \end{cases} \begin{cases} N = \frac{P}{2}\tan(\alpha) \end{cases} . \tag{3}$$

The equation for the deflection curve of the beam is

$$y'' = \gamma\left[-x - \tan(\alpha) \cdot y\right] \quad , \tag{4}$$

where $\gamma = \frac{1}{EI}\frac{P}{2}$, with the following boundary conditions:

$$y(0) = 0 \quad , \quad y'\left(\frac{L}{2}\right) = 0 \quad . \tag{5}$$

Then the solution of equation 4, satisfying the boundary conditions given by equation 5, is

$$y = \frac{\sqrt{2}}{\sqrt{\gamma \cdot \tan(\alpha)} \cdot \tan(\alpha) \cdot \cos\left(\sqrt{\gamma \cdot \tan(\alpha)} \cdot \frac{L}{2}\right)} \cdot \sin\left(\sqrt{\gamma \cdot \tan(\alpha)}\right) - \frac{x}{\tan(\alpha)} \quad . \tag{6}$$

The central deflection can be calculated using the equation 6 for $x = L/2$

$$y\left(\frac{L}{2}\right) = \frac{\sqrt{2}\tan\left(\sqrt{\gamma \cdot \tan(\alpha)} \cdot \frac{L}{2}\right)}{\sqrt{\gamma \cdot \tan(\alpha)} \cdot \tan(\alpha)} - \frac{L}{2\tan(\alpha)} \quad . \tag{7}$$

Finally the formula for the stress in the midspan outer fibres is obtained.

$$\sigma_r = \frac{3P}{B \cdot h^2}\left[\frac{L}{2} + \tan(\alpha)\left(\frac{\sqrt{2}\tan\left(\sqrt{\gamma \cdot \tan(\alpha)} \cdot \frac{L}{2}\right)}{\sqrt{\gamma \cdot \tan(\alpha)} \cdot \tan(\alpha)} - \frac{L}{2\tan(\alpha)}\right)\right] \quad . \tag{8}$$

The solution depends on the value of $\tan(\alpha)$ which is obtained by solving the following nonlinear equation:

$$\begin{aligned} y'(0) &= \frac{1}{\tan(\alpha) \cdot \cos\left(\sqrt{\gamma \cdot \tan(\alpha)} \cdot \frac{L}{2}\right)} - \frac{1}{\tan(\alpha)} \\ &= \tan(\alpha) \quad . \end{aligned} \tag{9}$$

Large deflections of the beam are related to changes in the span length and to slippage of the specimens at the supports [3]. Change in the span length takes place as a consequence of rotation of the beam on the supports when large deformation is induced, as is described in figure 3 for the case studied.

The changes in the distance L can be estimated as follows:

$$L \rightarrow L - 2a \quad , \quad a = \frac{d+h}{2} \sin(\alpha) \quad . \tag{10}$$

where d = diameter of pin support; h = thickness of the specimen.

The comparison of exact theory (ET) and the CLT with the experimental results lead to a correction of the length change for both theories.

$$L \rightarrow L - 2a \quad , \quad \begin{cases} a = \frac{d+2h}{2} \sin(\alpha) \quad , \quad \text{(ET)} \\ a = \frac{d-2h}{2} \sin(\alpha) \quad , \quad \text{(CLT)} \end{cases} \quad . \tag{11}$$

These corrections are empirical, without geometrical justification, and only proved to be valid for this particular case. The justification for the need of these empirical corrections can be given by two arguments. The first one is the change of the area where the central load is applied, which increases with the load. The second one is the accumulation of different types of internal damage in the laminates during the loading, which causes a decrease of the stiffness. In fact the decrease of the stiffness has been used as a measure of the damage by many researchers, as referred by Steif [4]. Obviously the empirical corrections may compensate the consequences of these phenomena.

In figure 4 the experimental maximum deflections in function of the load are plotted and compared quite well with the exact and corrected linear solutions.

In figure 5 the calculated maximum stresses in function of the load are plotted for the exact theory (ET), correct linear theory (CLT), the ASTM equation and the linear theory (LT). All cases match very well except, of course, the linear theory.

Only the exact solution can predict an instability condition, this results in the load reaching a maximum and falling thereafter [2] for:

$$P_{crit} \cdot \frac{L^2}{EI} = 6.72 \quad . \tag{12}$$

Using the previous analysis on the 3PB-test results, the flexural properties were calculated and are presented in the tables 5, 6 and 7.

Compared to tape laminates UC125 $[0^o\ /90^o\ ]_{4s}$, quasi-laminar textile composites CC194 $[0^o\ ]_{4s}$ with equal volume fractions of in-plane fibres had slightly lower in-plane stiffness. This is explained by the tow waviness in the textile composites [5]. The rupture load for the UC125 test specimens was always lower than the critical load given by equation 12, as shown in figure 6. In the case of the CC194 test specimens the rupture load was very closed to the critical load, pointing to a rupture due to geometrical instability. As a consequence the measured rupture stresses for the CC194 laminates are much lower than the value indicated by the supplier.

Alternatively this methodology can be used to measure the damage by recalculating the modulus each time, instead of using the empirical correction given by equation 11. The modulus decay given by the ratioE/E_b, where E is the instantaneous modulus, was calculated and is presented in tables 5, 6 and 7.

Creep test apparatus

Due to limitations on temperature control device inside the laboratory, an environmental chamber was used. Inside the chamber the temperature and the normalised humidity was maintained steady.

In figure 7 the test apparatus is shown inside the environmental chamber. The maximum applied stresses were always lower than 10% of the rupture stress. A close view of test apparatus with the respective geometry is also shown in figure 8.

The creep extensions were measured using electrical strain gauges, HBM 10/350LY41. For the bending tests, the tensile and compression extensions are recorded close to the section of maximum bending moment. A Personal Computer controlled data acquisition board, SOLARTRON 3595, was used to automatically record the experimental data.

The conventional foil electrical resistance strain gauges used in these tests displayed the required sensitivity characteristics but were unstable over a long term. In order to smooth out extraneous noise without altering the data characteristics and compact data into a smaller set the following procedure [6] was used:

For each decade, in logarithmic time scale, the data was divided in ten equal time intervals;

The data in each time interval was fitted into a single term exponential,

$$\epsilon = A \cdot e^{B \cdot t} \quad , \tag{13}$$

where ϵ = the strain response; t = time; A and B = best fit constants by least squares method;

The entire n data points in each time interval was replaced by $\overline{\epsilon}$ and $\overline{t}$:

$$\overline{t} = \frac{\sum_{i=1}^{n} t_i}{n} \quad , \quad \overline{\epsilon} = A \cdot e^{B \cdot \overline{t}} \quad . \tag{14}$$

Dynamic-Mechanical-Thermal-Analyser (DMTA) test result

The characterisation of the mechanical properties of polymeric materials on a DMTA analyser gives the complex compliance ($S*$) as a function of angular frequency w. In order to characterise the viscoelastic material behaviour in a very broad range of frequencies (or times), it is necessary to combine measurements at several temperatures applying the time-temperature superposition principle (TTSP). According to this principle, a given property measured for short times must be identical with one measured for longer times at a lower temperature, so, the curves are shifted parallel to the horizontal axis matching to form a master curve.

The dynamic test specimens were cutted out from plates with three different stacking sequences. The dynamic tests were carried out in a beam cantilever apparatus. The specimens had a thickness of $2.2mm$, width of $10.0mm$ and the distance between the support and the load application point of $22.0mm$.

A brief description of the methodology used to obtain the creep master curves [7] is given. For each temperature level, the frequencies varied from

$0.1Hz$ to $100Hz$. The maximum imposed deflection was $64\mu m$ and the temperature levels were within the range of $20°C$ to $135°C$. Following the frequency-time transformation procedure, the short-term compliance curves in time domain were obtained. Then the data was shifted for each temperature to a reference temperature, T_{ref}, using the time-temperature superposition principle (TTSP) to build up the master creep compliance curve as shown in figure 9.

Many authors already discussed the inaccuracy of the simple power law to model the whole master curve. The Simple Power Law is defined as follows:

$$S(t) = S_0 + S_1 \left(\frac{t}{\tau_0}\right)^n \tag{15}$$

where S_0 = time independent initial compliance; S_1 = coefficient of the time dependent compliance; n = material constant; and τ_0 = unit reference time.

Many polymers, such as the crosslinked polymers, deform in an asymptotic form, from glassy to rubber like behaviour. In the literature there are many expressions of the time-dependent compliance that can describe the viscoelastic phenomena over a broad range. In this study the response function [8] chosen to fit the master curve was given by:

$$\frac{S(t)}{S_0} = 1 + \frac{S_\infty - S_0}{S_0} w(t) \tag{16}$$

where $w(t)$ is the Cole-Cole function

$$w(t) = \frac{1}{1 + \left(\frac{\tau_0}{S_0}\right)^n} \tag{17}$$

where S_0 = time independent initial compliance; S_∞ = time independent compliance at infinity time; n = material constant; and τ_0 = unit reference time.

The master curves were fitted to the Cole-Cole function but it was found that the curve fitting didn't have a good agreement in the longer time range. The curve fitting and the fitting results are shown in figure 9 and in table 8.

The discrepancy in the longer time range was related to the shape of the compliance master curves. Although the master curves shown a decrease of the creep at longer times, it was clear that they did not reach a limit value as the Cole-Cole function predicts. Nevertheless, if the working temperatures are lower than 50^oC, then the longer time range, 106 to 1014 hours, represents very long times, i.e., 114 and 11.4 billions of years, respectively. Hence, in this case, it is perfectly reasonable to use the Simple Power Law to predict long-term behaviour in a human time scale, i.e., 50 years.

Creep test results

The creep compliance is defined as:

$$S(t) = \frac{\epsilon(t)}{\sigma_0} \tag{18}$$

where $\epsilon(t)$ = strain measured; σ_0 = constant stress imposed ; $S(t)$ = creep compliance.

For a better comparison of all test specimens the normalised creep compliance was used instead of the creep compliance. The normalised creep compliance is defined as:

$$S_R(t) = \frac{S(t)}{S_0} \tag{19}$$

where $S(t)$ = creep compliance; S_0 = the instantaneous compliance $S_R(t)$ = normalised creep compliance.

After almost 1800 hours of bending creep test of specimens made of UC 125 RNA at 23^oC and $50\%Hr$, no significant creep strains were detected within the strain gauges accuracy, i.e., $\pm$ $20\mu m$.

These results motivated the decision to increase the temperature to 50^oC instead of increasing the loading stress, with two purposes: accelerate the viscoelastic behaviour and avoid the non-linear behaviour.

In figures 10 and 11 the creep test results are plotted with the simple power law predictions (Findley) and the master creep curve (DMTA). All experimental results are in tension except the B2(C) and C5(C) that are in compression. The Findley or the simple power law was already defined by equation 15.

These experimental results, representing more than 2500 hours, revealed an increase of the creep compliance around 6.7% in average for the CC194 and around 2.5% in average for the UC125. Surprisingly the creep tests pointed that the CC194 has a larger increase of the creep compliance than the UC125. For continuous carbon fibre composites, the time dependency exhibited by the fibre dominated mechanical properties E_{11}, ν_{12} is negligibly small, when compared to the highly time dependent matrix dominated properties. Then, for these staking sequences no significant creep was expected due to the existence of fibres in the loading direction.

At this stage some conclusions can be addressed. The results showed a large discrepancy between the DMTA and the bending creep, apparently having distinct behaviours. In fact each test involved specimens with different dimensions but the scale factor, alone, could not explain so large deviations. On the other hand the Findley equation prediction for the CC194 specimens, based on the first 100 hours , shown a good agreement with the experimental data until the 1000 hours were reached. After this time the creep data shown a large decrease of the creep rate, apparently diverging from the power law. As for the UC125 specimens the predictions of the Findley are in good agreement with the experimental data, certainly due to the very low creep level presented. Having this in mind a new model was developed.

Analysis of experimental results using a new model

The new model approach was developed after a careful analysis of the DMTA test apparatus. It was not difficult to conclude that the beam cantilever should be considered a short beam. Therefore it becomes obvious that the DMTA results were related not only with the compliance but also with the shear compliance of the laminate. For that very reason the properties of the viscoelastic matrix could only be determined approximately.

The Poisson's ratio υ^m of the viscoelastic matrix was considered constant and equal to 0.25. The creep compliance $S^m = S^m_{11} = S^m_{22}$ and the shear creep compliance S^m_{66} of the matrix were calculated using some approximations. In this case it was considered that the DMTA test measured, directly, the shear creep compliance of the laminate admitting that the influence of the creep

compliance of the laminate could be ignored, i.e., $S_{11}(t) \approx 1/E_b$. The equation 20 gives the relation between the creep compliance, obtained directly from DMTA tests, and the shear creep compliance of the laminate. The equation 20 was obtained by comparison of beam cantilever solution with and without the shear correction.

$$S_{66}(t) = \frac{1}{6}\left(\frac{L}{h}\right)^2 \left(\bar{S}(t) - \frac{1}{E_b}\right) \tag{20}$$

where L = the length of the beam; h = the thickness of the laminate; $\bar{S}(t)$ = the creep compliance obtained from the DMTA and E_b = the bending modulus of the laminate considered linear elastic.

The micromechanics formulae based on the Halpin-Tsai equations had been adapted and used for viscoelastic analysis [9], [10]. Based on such analysis, assuming the fibres linear elastic and the woven composite as a multidirectional laminate consisting of the fibre angles, the relationship between shear creep compliance of the matrix, $S_{66}^m(t)$, and the laminate shear creep compliance, $S_{66}(t)$, was obtained as follows:

$$\begin{aligned} S_{66}^m(t) &= \frac{1}{2(1-\nu_f)}\left\{\left(S_{66}(t) - S_{66}^f\right)\cdot(1+\nu_f) + \right. \\ &\quad + \left[\left(S_{66}(t)\right)^2\cdot(1+\nu_f)^2 + S_{66}(t)\cdot S_{66}^f\cdot\left(2-12\nu_f+2\nu_f^2\right) + \right. \\ &\quad \left.\left. + \left(S_{66}^f\right)^2\cdot(1+\nu_f)^2\right]^{\frac{1}{2}}\right\} \end{aligned} \tag{21}$$

where ν_f = the volume fraction of the fibre; S_{66}^f = fibre shear compliance considered linear elastic and equal to 22 GPa [5].

Finally using a relation applied successively elsewhere [10] the creep compliance of the matrix was determined by the following equation 22.

$$S^m(t) = \frac{S^m_{66}(t)}{2(1+\nu^m)} \tag{22}$$

A nonlinear viscoelastic analysis of the carbon fibre matrix interphase was already presented by another researcher [11]. The present approach considers a viscoelastic interlayer between each ply of the laminate, i.e., a resin-rich interlayer zone with the same properties of the resin, with a thickness to be determined, as shown in figure 12.

Introducing the geometry and properties of the laminates into the LAMFLU program [12], it was possible to determine approximately the resin interlayer thickness, unknown at this stage, for the UC125 and CC194 laminates using the first 100 hours of the experimental results. The results for the interlayer thickness, see figure 12, are presented on table 9.

The values determined for the interlayer thickness reveal that the twill woven laminate (CC194) has a larger resin interlayer, i.e., 44% of the ply thickness, than the tape laminate (UC125).

The woven composites compared to tape laminates, with the same volume fractions of in-plane fibres, have usually slightly lower in-plane stiffness because of the tow waviness. Therefore, axial shear stresses are higher under nominally aligned loads [5]. The tow waviness and the higher shear stress could justify the larger resin interlayer thickness of the CC194 in the present model.

The analysis of delamination in angle-ply composites lead some researchers [13] to model the composite laminate as an assembly of anisotropic homogeneous plies bonded by thin resin interlayers. The interlaminar resin layer was considered an isotropic material with a uniform thickness of one-tenth of the individual ply thickness as observed under microscope [14].

In the present case no microscopic observations were made but it was clear that the present model was a crude simplification of the real resin interlayer of the CC194 laminate. Probably the interlayer thickness that was determined for the present model reflected the influence rather the real geometry of the viscoelastic interlayer.

In figures 13 and 14 the predictions of the present model (Model) and of the simple power law (Findley) are plotted with the averaged experimental data (Exper.). The predictions made by LAMFLU (Model) compared reasonably well with the experimental results. The model predicts a limit to the creep deformation and the experimental data appears to follow the same trend.

The laminate plies were considered linear elastic for the CC194 and the UC125. In fact the UC125 is not really unidirectional, i.e., contains glass fibres in the weft directions, about 20% in weight. Therefore the viscoelastic interlayers suffer creep and stress relaxation simultaneously and as a consequence originate load transfer to the adjacent layers. After a certain period of time an equilibrium state is reached and the creep deformation is arrested.

Conclusions

The methodology to design highly stable structures followed by CERN lead to choose CFRP laminates as structural elements. The creep behaviour of a quasi laminar textile and an equivalent tape laminate was compared.

The initial analysis pointed the twill woven laminate as a better choice in a long-term behaviour basis. The experimental creep tests showed a different picture, the tape laminates exhibited lower creep strains than the twill woven laminates and proven to be more stable. The simple power law was adequate to fit the UC125 and CC194 experimental data for the first 100 hours. The model extrapolations for the UC125 laminates showed a good agreement with the experimental results. For the CC194 laminates the model extrapolation shown a good agreement until 1000 hours were reached, after this the model diverged from the experimental results. The experimental data for the CC194 laminates shown an evolution of the creep strain to a limit value near 2000 hours.

One simple explanation for CC 194 behaviour, which came out initially, was found on the reinforcement tissue itself. The overlap of the transverse and longitudinal fibres (twill woven) could produce plies with fibres not stretched. The tensile stresses and the viscoelastic matrix then promoted the stretching of the fibres. This phenomenon should not happen in unidirectional reinforcements. Nevertheless this paradigm did not seem satisfactory to explain the experimental results.

The creep master curves obtained from the dynamic mechanical and thermal analysis (DMTA) were very similar for both laminates UC125 RNA [0^o /90^o

]4s and CC 194 RNA [0^o]4s. The master curves shown an increase of the creep compliance (to a limit value?) between 16 and 19 times of the initial value. Further the master curves indicate, as shown in figure 9, that it takes an absurd time to reach this limit at 50^oC, i.e., 1 millions of years!

One the other hand the comparison of creep master curves and creep test results have shown a large discrepancy. A new interpretation of the DMTA results was done. This allowed the determination of the matrix viscoelastic properties using the micromechanic analysis. The introduction of a viscoelastic interlayer between plies into the laminate model resulted into a new approach. The developed model explained the experimental results and permitted a long-term prediction of the creep bending response of the UC125 RNA $[0^o\ /90^o\ ]_{4s}$ and CC 194 RNA $[0^o\ ]_{4s}$ laminates based on Time Temperature Superposition Principle.

References

1. R. M. Guedes, A. T. Marques, and A. H. Cardon, Creep/Creep-Recovery Response of Fibredux 920C-TS-5-42 Composite under Flexural Loading, *Applied Composite Materials* **6**, pp. 71–86, 1999.

2. J. Williams, *Stress Analysis of Polymers*, pp. 160–173. Mechanical Engineering, Ellis Horwood, 1980.

3. Y. M. Tarnolpols'skii and T. Kincis, *Static Test Methods for Composites*, ch. 5, pp. 220–263. Van Nostrand, Reinhold, New York, 1985.

4. P. S. Steif, Stiffness Reduction Due to Fiber Breakage, *Journal of Composite Materials* **17**(2), pp. 152–172, 1983.

5. B. Cox and G. Flanagan, Handbook of Analytical Methods for Textile Composites, Tech. Rep. 4750, NASA, 1997.

6. E. M. Wu, N. Q. Nguyen, and R. L. Moore, Matrix-Dominated Time-

Dependent Deformation and Damage of Graphite/ Epoxy Composite Experimental Data Under Ramp Loading, Tech. Rep. AFWAL-TR-82-3076, Lawrence Livermore National Laboratory, Livermore, California, 1982.

7. R. M. Guedes, A. T. Marques, and A. H. Cardon, Creep or Relaxation Master Curves Calculated from Experimental Dynamic Viscoelastic Function, *Science and Engineering of Composite Materials* **7**(3), pp. 259–267, 1998.

8. Q. Yang, *Nonlinear Viscoelastic-Viscoplastic Characterization of a Polymer Matrix Composite.* PhD thesis, Free University of Brussels (V.U.B.), 1996.

9. S. W. Beckwith, Viscoelastic Characterization of a nonlinear, glass/epoxy composite using micromecanics theory, in *JANNAF*, Structures and Mechanical Behaviour Working Group Meet., San Francisco, CA, February 1975.

10. A. Horoschenkoff, Characterization of the Creep Compliances J22 and J66 of Orthotropic Composites with PEEK and Epoxy Matrices Using the Nonlinear Viscoelastic Response of the Neat Resins, *Journal of Composite Materials* **24**, pp. 879–891, August 1990.

11. E. Sancaktar and P. Zhang, Nonlinear Viscoelastic Modelling of the Fiber-Matrix Interphase in Composite Materials, *Journal of Mechanical Design* **112**, pp. 605–619, 1990.

12. R. M. Guedes, A. T. Marques, and A. H. Cardon, Analytical and Experimental Evaluation of Nonlinear Viscoelastic-Viscoplastic Composite Laminates under Creep, Creep-Recovery, Relaxation and Ramp Loading, *Mechanics of Time-Dependent Materials* **2**, pp. 113–128, 1998.

13. S. Wang, An Analysis of Delamination in Angle-Ply Fiber-Reinforced Composites, *Transactions of the ASME* **47**, pp. 64–70, 1980.

14. C. Wu, Nonlinear Analysis of Edge Effercts in Angle-Ply Laminates, *Computers & Structures* **25**(5), pp. 787–798, 1987.

Table 1: Geometry of test specimens from plate UC125 RNA $[0^o$ /45^o /90^o /-45^o $]_{2s}$

Specimens	**A1**	**A2**	**A3**	**A4**
h (mm)	2.32	2.36	2.35	2.32
B (mm)	48.87	50.08	50.42	49.51

Table 2: Geometry of test specimens from plate UC125 RNA $[0^o$ /90^o $]_{4s}$

Specimens	**B1**	**B2**	**B3**
h (mm)	2.32	2.36	2.35
B (mm)	48.87	50.08	50.42

Table 3: Geometry of test specimens from plate CC194 RNA $[0^o$ $]_{4s}$

Specimens	**C4**	**C5**	**C6**	**C7**
h (mm)	2.00	2.02	2.01	2.02
B (mm)	48.91	49.22	48.28	47.26

Table 4: Layer elastic properties of the laminates

Specimens	$\mathbf{E_1}$**(GPa)**	$\mathbf{E_2}$ **(GPa)**	$\boldsymbol{v}_{12}$	$\mathbf{G_{12}}$**(GPa)**
UC125 RNA	92.05	11.69	0.25	3.74
CC194 RNA	53.57	53.57	0.058	3.82

Table 5: Static bending properties of the test specimens UC125 $[0^o$ /45^o /90^o /-45^o $]_{2s}$

Specimens	**A1**	**A2**	**A3**	**Average**
E_b (GPa)	38.84	38.57	39.07	38.83
σ_r (MPa)	653	648	624	642
$E/E_b(\%)$	95.5	96.7	94.2	95.5

Table 6: Static bending properties of the test specimens UC125 $[0^o$ /90^o $]_{4s}$

Specimens	**B1**	**B2**	**B3**	**Average**
E_b (GPa)	46.76	46.72	48.72	47.40
σ_r (MPa)	850	850	865	855
$E/E_b(\%)$	93.5	91.2	92.4	92.4

Table 7: Static bending properties of the test specimens CC194 $[0^o$ $]_{4s}$

Specimens	**C1**	**C2**	**C3**	**Average**	**Supplier**
E_b (GPa)	41.94	42.50	42.16	42.20	50
σ_r (MPa)	717	727	731	725	900
$E/E_b(\%)$	92.5	91.4	91.6	91.8	

Table 8: Parameters of the master complince curve

Parameters	n	$\boldsymbol{\tau}_0$	$(S_\infty - S_0)/S_0$
UC125	0.32	5×10^5	13.47
CC194	0.32	12×10^5	15.15

Table 9: Thickness of the plies and the resin interlayers

Dimensions (mm)	h_p	h_i	h_p/h_i (%)
UC125	0.1438	0.0296	21
CC194	0.2500	0.1086	44

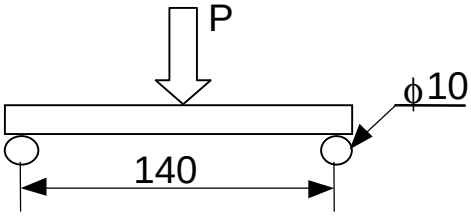

Figure 1: The geometry of the three point bending tests (3PB)

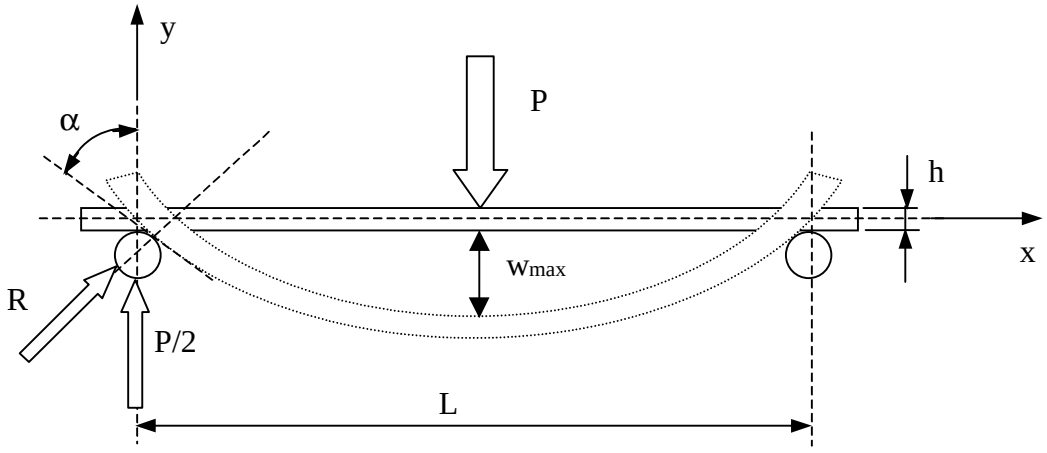

Figure 2: A three point bending test (3PB) with large deflections

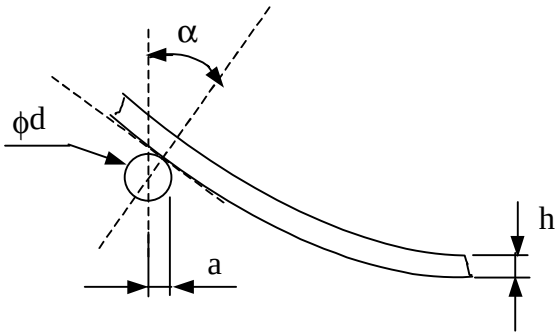

Figure 3: The change in the span length for the simply supported beam with a central load

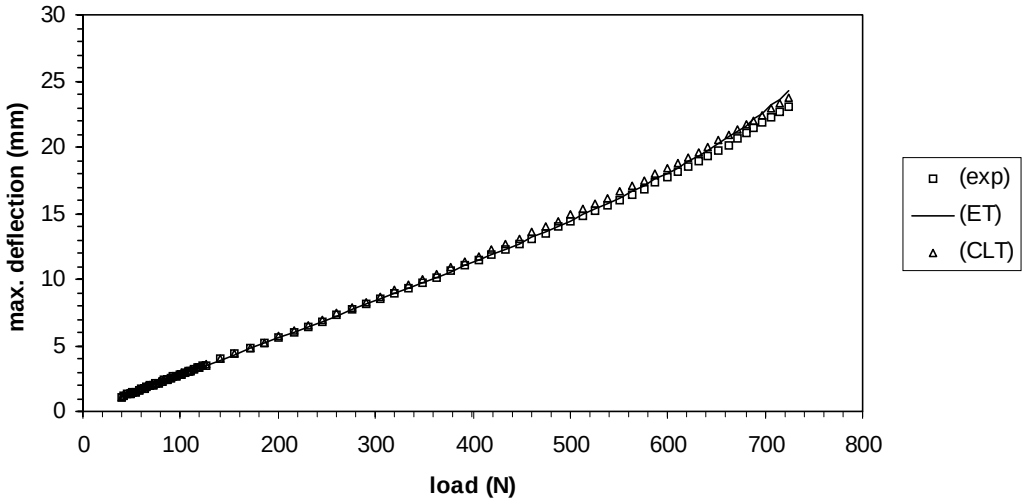

Figure 4: The deflection at the midspan for the 3PB tests compared with analytical solutions

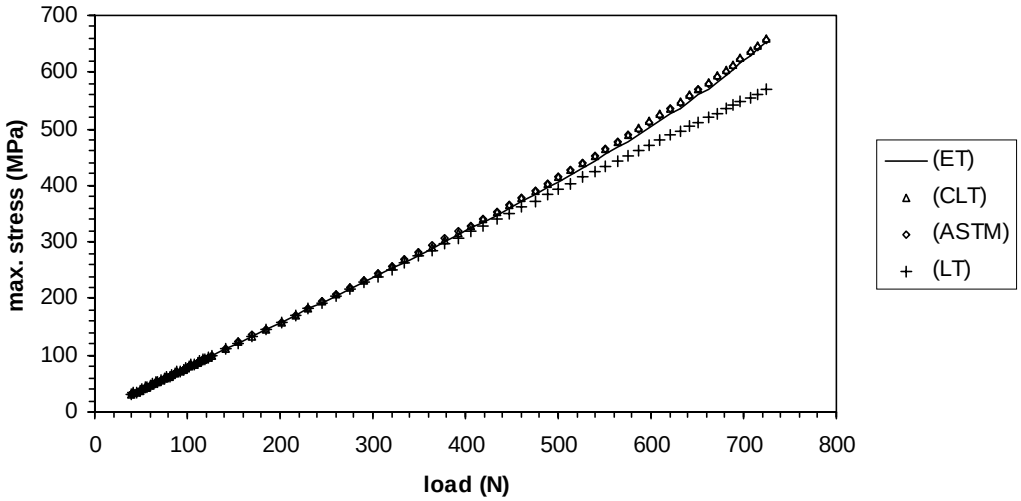

Figure 5: The maximum stress calculated at the midspan for the 3PB tests for several theories

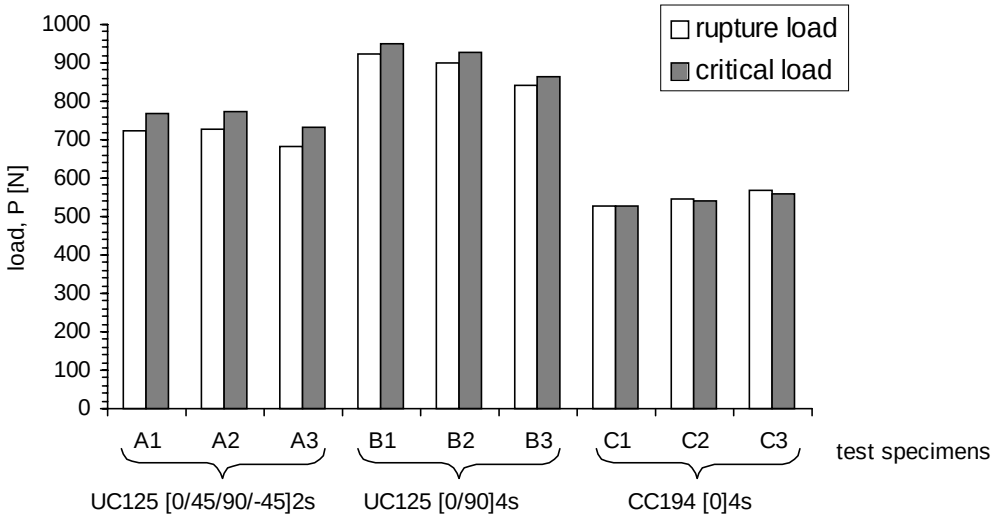

Figure 6: Comparison of rupture and critical load for the 3PB rupture tests

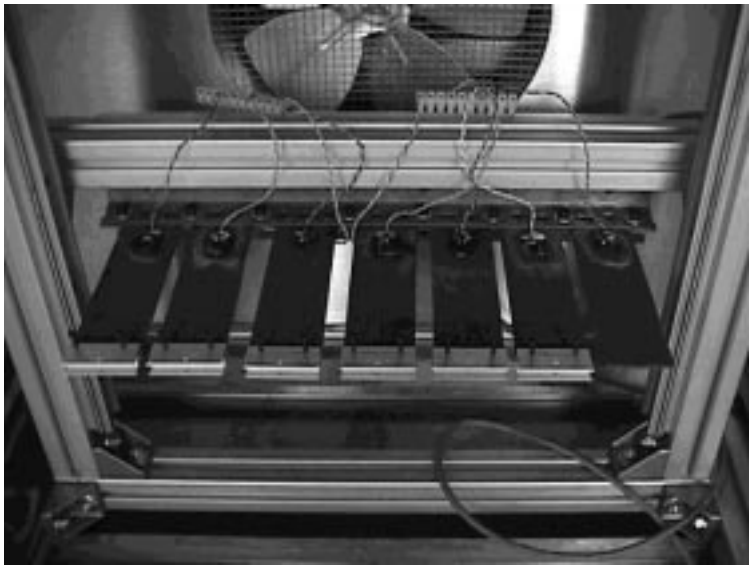

Figure 7: Test apparatus inside the environmental chamber

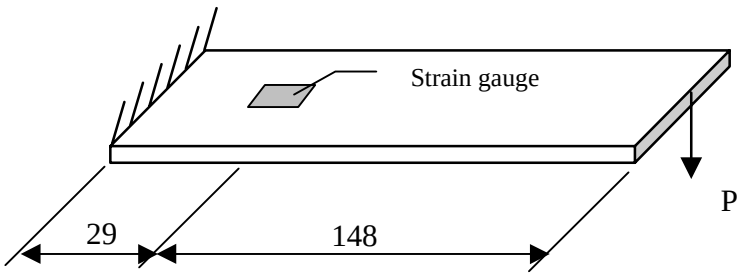

Figure 8: The test geometry and position of the strain measuring point

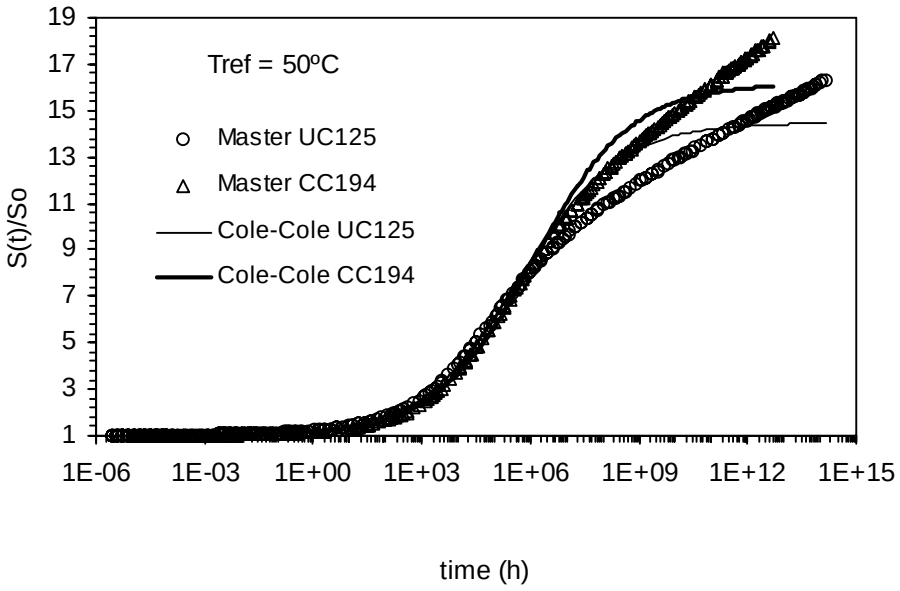

Figure 9: Normalized creep compliance master curves

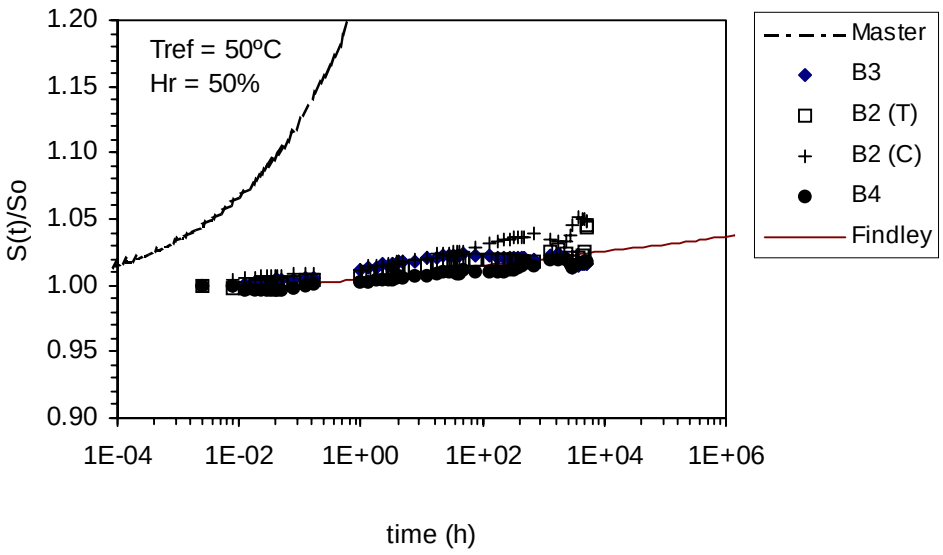

Figure 10: Normalized creep compliance for the UC125 RNA $[0^o/90^o]_{4s}$ test specimens

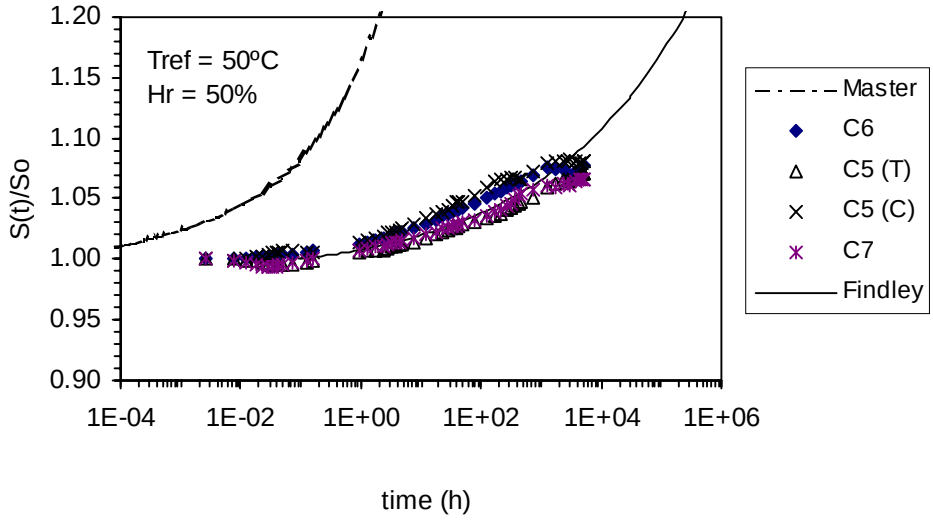

Figure 11: Normalized creep compliance for the CC 194 RNA $[0^o]_{4s}$ test specimens

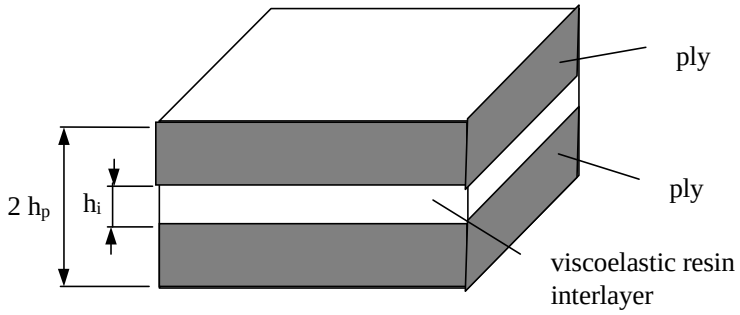

Figure 12: Laminate detail of the viscoelastic resin interlayer

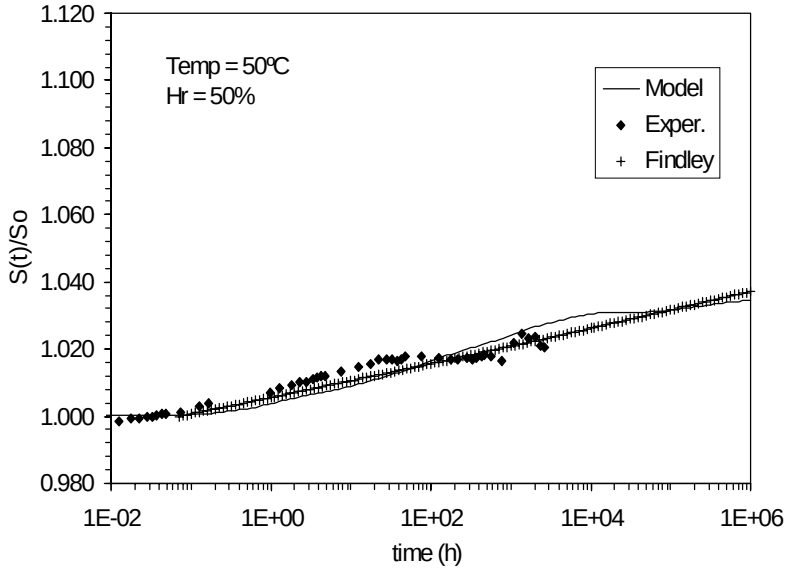

Figure 13: The averaged creep compliance of the UC125 RNA $[0^o/90^o]_{4s}$ test specimens with the model and Findley predictions

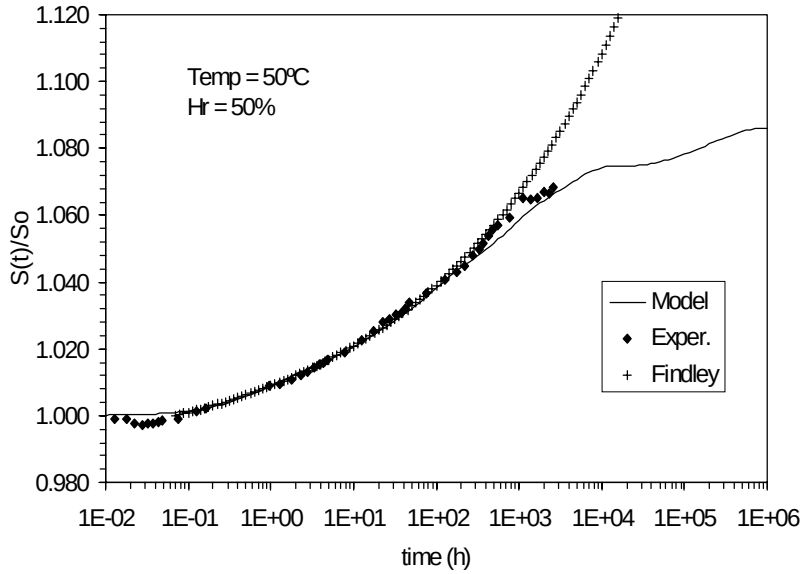

Figure 14: The averaged creep compliance of the CC194 RNA $[0^o]_{4s}$ test specimens with the model and Findley predictions